

Using Molecular Simulation to Understand the Structure of $[\text{C}_2\text{C}_1\text{im}]^+$ –Alkylsulfate Ionic Liquids: Bulk and Liquid–Vapor Interfaces

Xavier Paredes,[†] Josefa Fernández,[†] Agílio A. H. Pádua,[‡] Patrice Malfreyt,^{*,‡} Friedrich Malberg,[§] Barbara Kirchner,[§] and Alfonso Sanmartín Pensado^{*,†,§}

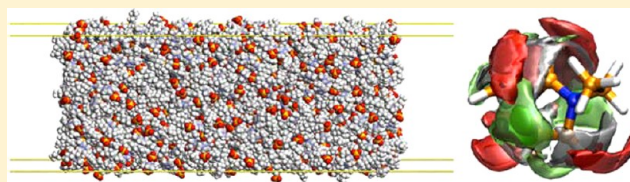
[†]Laboratorio de Propiedades Termofísicas, Departamento de Física Aplicada, Universidade de Santiago de Compostela, E-15782 Santiago de Compostela, Spain

[‡]Institut de Chimie de Clermont-Ferrand, Equipe Thermodynamique et Interactions Moléculaires, Clermont Université, Université Blaise Pascal, BP 80026, 63171 Aubiere, France, and CNRS, UMR6296 ICCF, BP 80026, F-63171 Aubiere, France

[§]Wilhelm-Ostwald-Institut für Physikalische und Theoretische Chemie, Universität Leipzig, Linnéstrasse 2, D-04103 Leipzig, Germany

Supporting Information

ABSTRACT: Using molecular dynamics simulations we have studied the structure of alkylsulfate-based ionic liquids: 1-ethyl-3-methylimidazolium *n*-alkylsulfate $[\text{C}_2\text{C}_1\text{im}][\text{C}_n\text{SO}_4]$ ($n = 2, 4, 6$ and 8). The structure of the different ionic liquids have been interpreted taking into account radial and spatial distribution functions, and structure factors, that allowed us to characterize the morphology of the polar and nonpolar domains present in this family of liquids. The size of the nonpolar regions depends linearly on the anion alkyl chain length. Furthermore, properties of the surface of ionic liquids, such as surface tension, ordering, and charge and density profiles, were studied using molecular simulation. We were able to reproduce the experimental values of the surface tension with a maximum deviation of 10%, and it was possible to relate the values of the surface tension with the structure of the liquid–vacuum interfaces. Microscopic structural analysis of orientational ordering at the interface and density profiles along the direction normal to the interface suggest that the alkyl chains of the anions tend to protrude toward the vacuum, and the presence of the interface leads to a strong organization of the liquid phase in the region close to the interface, stronger when the side-chain length of the anions increases.



■ INTRODUCTION

The most accurate definition of ionic liquids (ILs) has been proposed by Hallett and Welton¹ quite recently: “Ionic liquids are compounds constituted entirely of ions, with melting points lower than 373 K”. No more general comments hold for ionic liquids; in addition the nature of the interactions present in this media are complex.^{2–6} Both cations and anions, usually voluminous and characterized by complex molecular structures, flexibility, high asymmetry and with delocalization of the electrostatic charge, can be selected to tune the physicochemical properties of the ILs. One of the most common statements on ionic liquids was that ionic liquids are nonvolatile, even though in 2002 Morrow and Maginn,⁷ with the aid of molecular simulation, predicted enthalpies of vaporization for ionic liquids in the range of 150–240 kJ·mol^{–1}. Then, Rebelo, Magee, and co-workers^{8,9} provided experimental evidence of the ability of ionic liquids to be distillable, opening intense research into the vapor phase of ionic liquids. Advances in the field of ionic liquids technology will strongly benefit a comprehensive understanding of both their bulk and surface properties. A wide range of chemical reactions takes place mainly at interfaces.¹ The use of ionic liquids in electrochemical applications^{10–12} and gas-storage techniques^{13–16} or gas

separation^{17–20} requires also an accurate description at the molecular level of the gas–liquid interfaces. Applications such as the synthesis of metallic nanoparticles^{21–24} will depend upon both surface and bulk properties. The size distributions of the nanoparticles²⁵ synthesized in different ionic liquids are related to the heterogeneous structure of the particular IL, which may contain polar and nonpolar regions.

Alkylsulfate-based ILs with a cation derived from imidazolium^{26,27} can be considered as some of the most promising ILs for application in industrial processes. In general, they can be easily synthesized in an atom-efficient and halide-free way, at a reasonable cost. They show low melting points,²⁸ relatively low viscosities,^{29,30} and high biodegradability. Thus, Deng et al.³¹ performed several toxicity and biodegradability studies on a large set of ionic liquids, observing that the ionic liquid $[\text{C}_1\text{COOC}_5\text{C}_1\text{im}][\text{C}_8\text{SO}_4]$ was completely degraded within 5 days; therefore, this IL can be considered “readily biodegradable” with the “CO₂ headspace test”. Wilfred et al.³² analyzed the performance of several ILs to efficiently remove sulfur

Received: September 25, 2012

Revised: October 22, 2012

Published: November 12, 2012

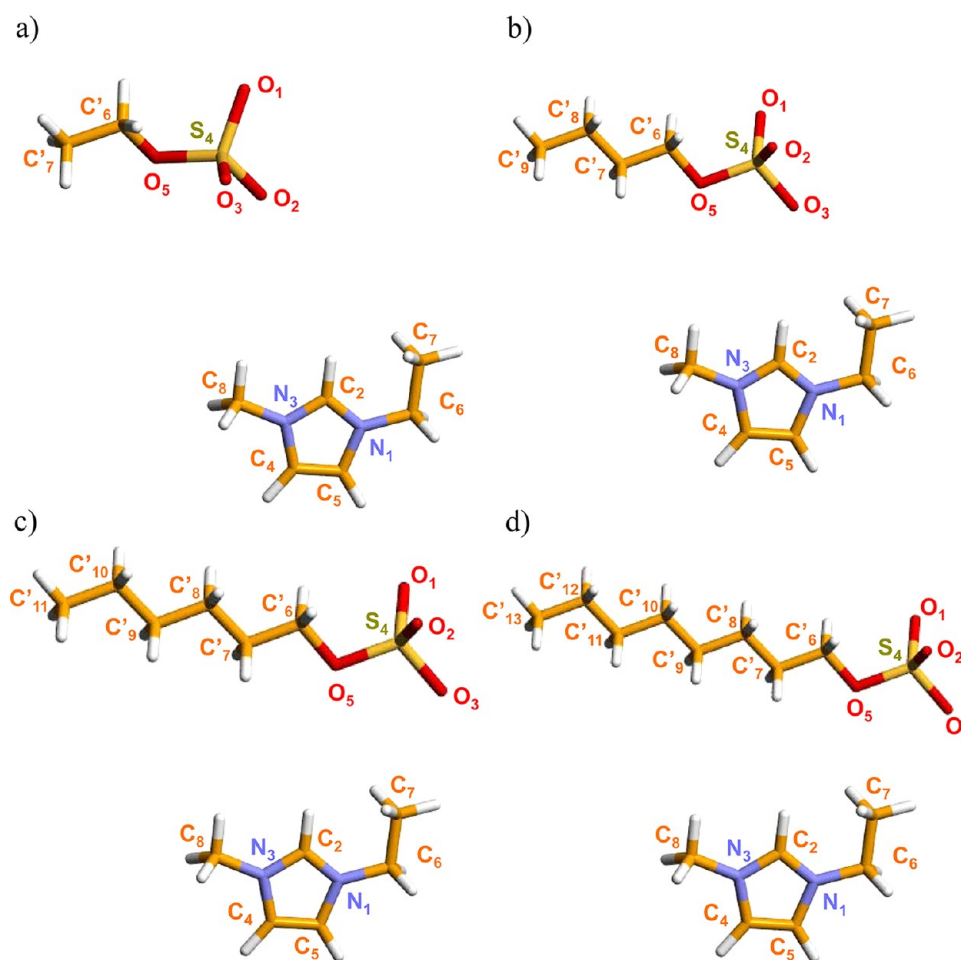


Figure 1. Adopted nomenclature for the sites of the studied ionic liquids. (a) 1-Ethyl-3-methylimidazolium ethylsulfate $[\text{C}_2\text{C}_1\text{im}][\text{C}_2\text{SO}_4]$, (b) 1-ethyl-3-methylimidazolium butylsulfate $[\text{C}_2\text{C}_1\text{im}][\text{C}_4\text{SO}_4]$, (c) 1-ethyl-3-methylimidazolium hexylsulfate $[\text{C}_2\text{C}_1\text{im}][\text{C}_6\text{SO}_4]$, and (d) 1-ethyl-3-methylimidazolium octylsulfate $[\text{C}_2\text{C}_1\text{im}][\text{C}_8\text{SO}_4]$.

compounds in oil refining. These authors investigated the effect of mass ratio between ILs and dodecane (model oil), extraction temperature, and extraction time on dibenzothiophene (DBT) removal efficiency. A total of 18 different ILs were used to extract DBT from dodecane respectively, observing that the ionic liquids $[\text{C}_4\text{C}_1\text{im}][\text{SCN}]$, $[\text{C}_4\text{C}_1\text{im}][\text{N}(\text{CN})_2]$, $[\text{C}_4\text{C}_1\text{im}][\text{C}_8\text{SO}_4]$, and $[\text{N}_{4441}][\text{CH}_3\text{CO}_3]$ were the top four ILs with desulfurization efficiency ranging from 66% to 62%. Pereiro et al.³³ studied the performance of the ionic liquid $[\text{C}_2\text{C}_1\text{im}][\text{C}_2\text{SO}_4]$ to separate azeotropic mixtures. This IL showed a high ability to act as an extraction solvent that allows purifying alkanes from their azeotropic mixtures with ethanol. Therefore, the development of new industrial applications of this family of ionic liquids will strongly benefit from a deep knowledge of both bulk and surface properties.

Russina et al.³⁴ have performed X-ray diffraction measurements on a range of ionic liquids based on the alkylsulfate anion, namely $[\text{C}_2\text{C}_1\text{im}][\text{C}_n\text{SO}_4]$, with $n = 2, 4, 6$, and 8 , that show the existence of nanoscale structural heterogeneities for all the ILs, with the size depending linearly on the anion alkyl chain length. Martinez et al.³⁵ combined sum-frequency generation spectroscopy, surface potential and surface tension measurements to analyze the ionic liquid–gas interface for 1-alkyl-3-methylimidazolium alkylsulfate ionic liquids, showing an increase on the surface potential of the IL when the length of the alkyl chain on the cation or anion increases. They also

conclude that the imidazolium ring and the sulfate group are found at the same distance from the surface for all the studied ILs.

In this work, we present results of MD simulations for the bulk phase of the ionic liquids 1-ethyl-3-methylimidazolium ethylsulfate $[\text{C}_2\text{C}_1\text{im}][\text{C}_2\text{SO}_4]$, 1-ethyl-3-methylimidazolium butylsulfate $[\text{C}_2\text{C}_1\text{im}][\text{C}_4\text{SO}_4]$, 1-ethyl-3-methylimidazolium hexylsulfate $[\text{C}_2\text{C}_1\text{im}][\text{C}_6\text{SO}_4]$, and 1-ethyl-3-methylimidazolium octylsulfate $[\text{C}_2\text{C}_1\text{im}][\text{C}_8\text{SO}_4]$, together with the study of the liquid–gas interface of the $[\text{C}_2\text{C}_1\text{im}][\text{C}_2\text{SO}_4]$ and $[\text{C}_2\text{C}_1\text{im}][\text{C}_8\text{SO}_4]$ ILs to assess the surface tension and the structure of the surface. This set of ionic liquids was chosen in order to rationalize the effect of increasing the side chain length of the anion in the bulk phase structure, the structure at the surface and the surface tension.

SIMULATION METHODOLOGY

Potential Model. Ionic liquids were represented by an all-atom force field,^{36,37} which is based on the AMBER/OPLS-AA framework^{38,39} but was developed specifically for ionic liquids. This model contains all the parameters required to simulate the alkylsulfate anions $[\text{C}_2\text{SO}_4]^-$, $[\text{C}_4\text{SO}_4]^-$, $[\text{C}_6\text{SO}_4]^-$, and $[\text{C}_8\text{SO}_4]^-$ and the 1-ethyl-3-methylimidazolium cation $[\text{C}_2\text{C}_1\text{im}]^+$ (Figure 1). The functional form of the force field contains four kinds of potential energy: stretching of covalent bonds, bending of valence angles, torsion around dihedral

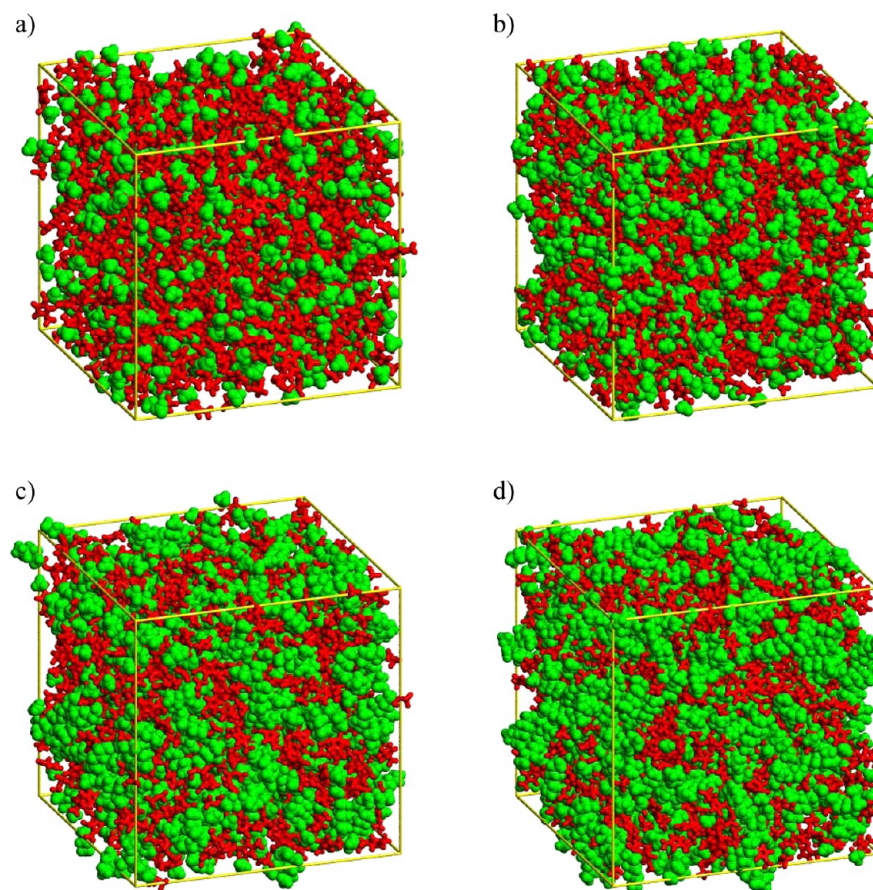


Figure 2. Snapshots of simulation boxes containing 512 ions of $[\text{C}_2\text{C}_1\text{im}][\text{C}_n\text{SO}_4]$, using a color code to identify the charged (polar) and nonpolar domains that form in ionic liquids. The lengths of the box sides are given: (a) $[\text{C}_2\text{C}_1\text{im}][\text{C}_2\text{SO}_4]$ $l = 54.7$ Å, (b) $[\text{C}_2\text{C}_1\text{im}][\text{C}_4\text{SO}_4]$ $l = 57.8$ Å, (c) $[\text{C}_2\text{C}_1\text{im}][\text{C}_6\text{SO}_4]$ $l = 60.4$ Å, and (d) $[\text{C}_2\text{C}_1\text{im}][\text{C}_8\text{SO}_4]$ $l = 63.0$ Å.

angles, and nonbonded interactions. Nonbonded interactions occur between atoms of the same molecule separated by more than three bonds and between atoms of different molecules. The potential energy associated with bonds and angles is described by harmonic terms, dihedral torsion energy is represented by a series of cosines, and nonbonded interactions are given by the Lennard-Jones sites and by Coulombic interactions (calculated using the Ewald summation method) between partial point charges placed on the atomic sites.

Computational Procedures. The bulk phase of the ionic liquids $[\text{C}_2\text{C}_1\text{im}][\text{C}_2\text{SO}_4]$, $[\text{C}_2\text{C}_1\text{im}][\text{C}_4\text{SO}_4]$, $[\text{C}_2\text{C}_1\text{im}][\text{C}_6\text{SO}_4]$, and $[\text{C}_2\text{C}_1\text{im}][\text{C}_8\text{SO}_4]$ were simulated in periodic cubic boxes containing 512 ion pairs using the molecular dynamics method implemented in the DL_POLY package.⁴⁰ The initial configurations were lattices with low density. Equilibrations starting from the low-density arrangement of ions took 1 ns, at constant NpT and $T = 423$ K, with a time step of 2 fs. Once the equilibrium density was obtained, simulation runs of 2 ns were performed. At the final densities of the ionic liquid state, the lengths of the sides of the simulation boxes range from approximately 54 Å to 63 Å for the ionic liquids with the $[\text{C}_2\text{SO}_4]^-$ and $[\text{C}_8\text{SO}_4]^-$ anion, respectively. Additionally, for the analysis of the free surfaces of the ionic liquid, we have considered rectangular parallelepiped simulation boxes of dimensions $L_x L_y L_z$ (with $L_x = L_y$) containing between 1024 ion pairs of the ionic liquids $[\text{C}_2\text{C}_1\text{im}][\text{C}_2\text{SO}_4]$ and $[\text{C}_2\text{C}_1\text{im}][\text{C}_8\text{SO}_4]$, for a total of around 30000 ($[\text{C}_2\text{C}_1\text{im}][\text{C}_2\text{SO}_4]$) and 50000 ($[\text{C}_2\text{C}_1\text{im}][\text{C}_8\text{SO}_4]$) atoms in the simulated systems.

Periodic boundary conditions were applied in the three directions of space. The direction normal to the surface of the ionic liquid was elongated (300 Å) so that the liquid slab occupies ~ 120 Å ($[\text{C}_2\text{C}_1\text{im}][\text{C}_2\text{SO}_4]$) and ~ 150 Å ($[\text{C}_2\text{C}_1\text{im}][\text{C}_8\text{SO}_4]$) in the middle with two equivalent interfaces. The systems were simulated via molecular dynamics using the DL_POLY program⁴⁰ at 423 K. The system was coupled to a Nosé–Hoover thermostat (constant NVT). The integration time step was 2 fs. Initial configurations were constructed by placing together two cubic boxes considered in the previous step. Equilibrations starting from this arrangement of ions took 1 ns (NpT), after which the systems were run for 1 ns to allow the interface to equilibrate. Then, a production run of 2 ns was executed. As expected, no detectable vapor phase was observed during the simulations. We calculated profiles of typical properties as a function of z (as the geometry of the system shows heterogeneity along the axis normal to the interface, z axis) by splitting the cell into slabs of width δz .

The methods used most frequently to calculate the surface tension^{41–43} consider the mechanical route definition and express the surface tension through the components of the pressure tensor. The Kirkwood and Buff expression⁴³ evaluates the components of the pressure tensor as a function of the derivative of the intermolecular potential. The definition of Irving and Kirkwood⁴² is based upon the notion of the force across a unit area and profit of expressing the local components of the pressure tensor along the direction normal to the interface. Gloor et al.⁴¹ have established a method based upon

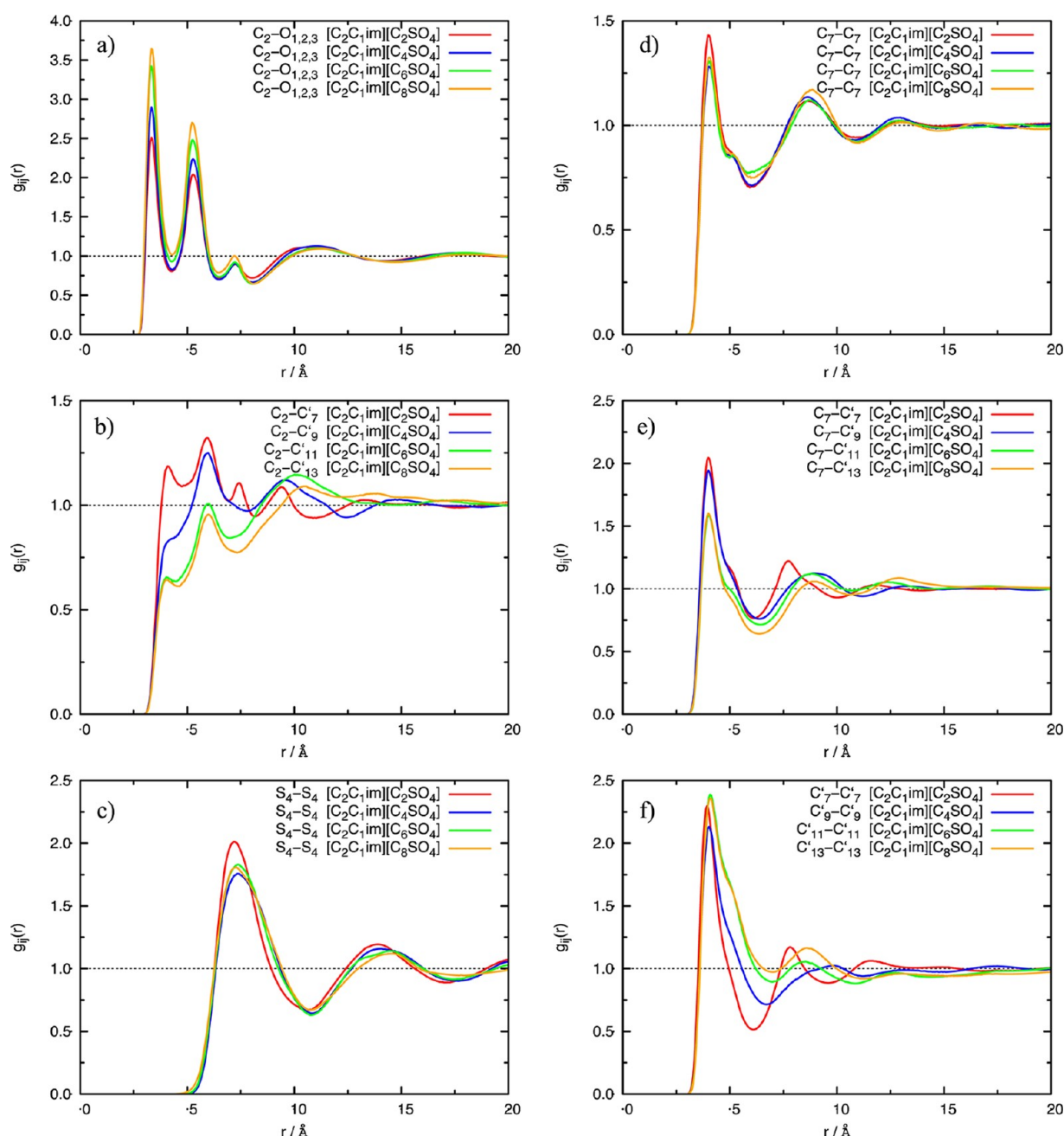


Figure 3. Cation–anion site–site radial distribution functions. (a) Oxygen atoms of the $[\text{C}_n\text{SO}_4]^-$ anions around the $[\text{C}_2\text{C}_1\text{im}]^+$ cation. (b) Terminal carbon atom of the $[\text{C}_n\text{SO}_4]^-$ anions around the $[\text{C}_2\text{C}_1\text{im}]^+$ cation. (c) Sulfur atom of the $[\text{C}_n\text{SO}_4]^-$ anions. (d) Terminal carbon atom of the $[\text{C}_2\text{C}_1\text{im}]^+$ cation. (e) Terminal carbon atom of the $[\text{C}_2\text{C}_1\text{im}]^+$ cation and terminal carbon atom of the $[\text{C}_n\text{SO}_4]^-$ anions. (f) Terminal carbon atom of the $[\text{C}_n\text{SO}_4]^-$ anions.

the thermodynamic definition of the surface tension allowing the calculation of this quantity through a perturbation of the cross-sectional area of the system containing the interface. In previous works, we have shown the equivalence of the three methods to assess the performance of the different routes to calculate the surface tension of ionic liquids.^{44,45} Full details of the calculation methods, including the treatment of long-range corrections, can be found elsewhere.⁴⁵

RESULTS AND DISCUSSION

Bulk Phase. Using molecular dynamics simulation, and almost simultaneously, Wang and Voth,⁴⁶ employing a multiscale coarse-graining (MS-CG) method, and Canongia

Lopes and Pádua,⁴⁷ using an all-atom potential model, reported the existence of a nanometer-scale structuring in imidazolium-based ionic liquids (from $[\text{C}_2\text{C}_1\text{im}]^+$ to $[\text{C}_{12}\text{C}_1\text{im}]^+$) corresponding to a segregation of polar and nonpolar domains. Ester-functionalized imidazolium-based ionic liquids⁴⁸ also present this characteristic nanosegregation in polar and nonpolar regions. Triolo and co-workers,^{34,49–52} using X-ray diffraction, provided experimental evidence of a nanoscale organization in the ionic liquids of the families $[\text{C}_n\text{C}_1\text{im}][\text{PF}_6]$, $[\text{C}_n\text{C}_1\text{im}][\text{BF}_4]$, $[\text{C}_n\text{C}_1\text{im}][\text{Cl}]$, $[\text{C}_n\text{C}_1\text{im}][\text{NTf}_2]$, and $[\text{C}_2\text{C}_1\text{im}][\text{C}_n\text{SO}_4]$. The importance of this segregation of the ionic liquids into polar (or ionic) and nonpolar spatial domains is a key issue to define their solvation characteristics, mainly

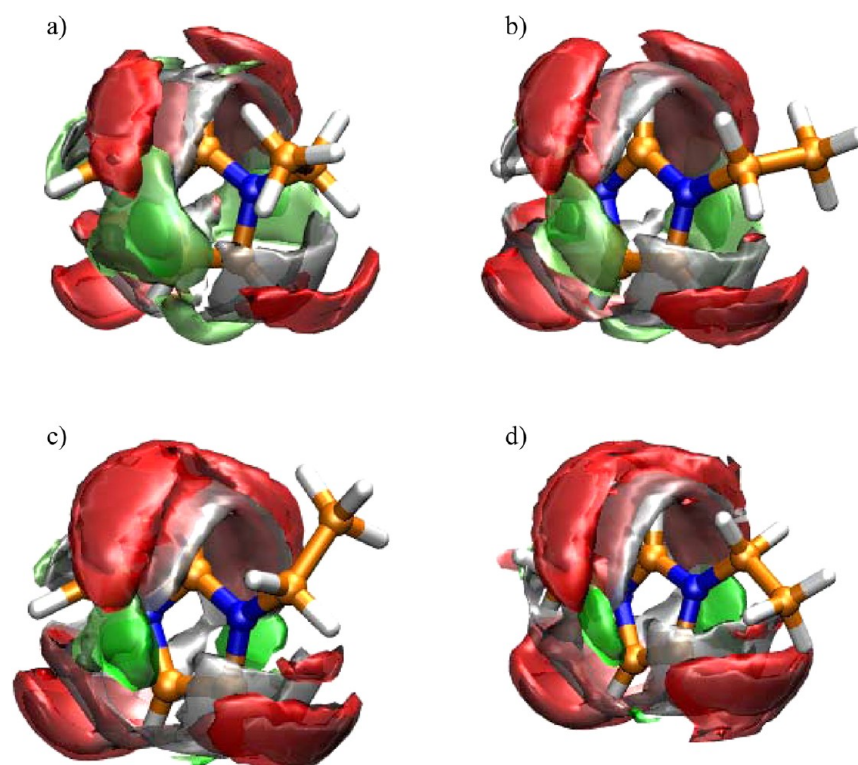


Figure 4. Spatial distribution functions of the oxygen atoms (gray: $O_{1,2,3}$, red: O_5), terminal atom of the anion (green) around the $[C_2C_1im]^+$ cation. (a) $[C_2C_1im][C_2SO_4]$, (b) $[C_2C_1im][C_4SO_4]$, (c) $[C_2C_1im][C_6SO_4]$ and (d) $[C_2C_1im][C_8SO_4]$. The isosurfaces represent 3 times the average density.

due to distinctive effects of this dual structure and also through the existence of different types of interaction with both polar and nonpolar solutes.⁵³

Figure 2 depicts the morphology of the polar and nonpolar regions for the studied alkylsulfate-based ionic liquids, using the same color code proposed by Canongia Lopes and Pádua⁴⁷ to identify high charge (red) and low charge density (green) regions. The polar regions considered to be of high charge density consist of the atoms of the imidazolium ring of the cation plus the atoms directly bonded to them (including the hydrogen atoms directly bonded to the first carbon of the alkyl chain), the sulfur and oxygen atoms of the alkylsulfate anions, together with the carbon atom bonded to the bridging oxygen atom, and the hydrogen atoms bonded to it. The terminal CH_3 group of the ethyl side chain of the cation and the remaining atoms of the side chain of the anions constitute the regions considered to be of low charge density (green). The distribution of the charged domains is not homogeneous but it has the form of a continuous tridimensional network of ionic channels that coexist with the nonpolar domains. The nonpolar domains form a dispersed phase in the case of the ionic liquid with the $[C_2SO_4]^-$ anion, whereas in the case of the IL with the $[C_8SO_4]^-$ anion the nonpolar domains form a continuous and complex tridimensional structure.

The snapshots of the simulation boxes depicted in Figure 2 present a qualitative (visual) description of the nanostructure of the considered ionic liquids; a more quantitative analysis can be performed by means of the radial distribution functions (RDFs) and the static structure factors, which can be directly compared with X-ray measurements. Figure 3 shows the site–site radial distribution functions between several representative atoms of the anions and cations of the studied ionic liquids. A prominent

feature of the RDFs is the strong correlation between the terminal oxygen atoms of the alkylsulfate anions and the atoms of the imidazolium ring of the $[C_2C_1im]^+$ cation. We observe larger peaks in the $C_2-O_{1,2,3}$ radial distribution functions when increasing the side chain of the anion, reflecting a more structured liquid phase. We also observe a strong peak in the S–S RDF (panel c, Figure 3) at distances around 7.5 Å, that correspond to conformations where two anions are linked to the same cation. For the ionic liquid $[C_2C_1im][C_2SO_4]$ the terminal atom of the side chain of the anion is also located close to the imidazolium ring (see panel b of Figure 3). Panels d–f of Figure 3 show the radial distribution functions between the terminal atoms of the cations and anions. The most remarkable feature is that the terminal atoms of both cations and anions tend to stick together, being the origin of the polar and nonpolar segregation present on the ionic liquids. Canongia Lopes and Pádua⁴⁷ observed for the family of ionic liquids $[C_nC_1im][PF_6]$ clear differences between the RDFs of the terminal atoms of the cations with the increase of the side chain, whereas in this work, the differences on the radial distribution functions of the terminal atoms of the investigated anions show small differences, highlighting how the molecular structure of the IL affects the structure of the liquid phase. We observe a shift of the first minimum of the RDFs, but the position of the first maximum, as well as its value is only slightly affected. We observe that the peak of the RDF between the terminal atom of the cation and the terminal atom of the anion decreases with the side-chain length. The structural features are better depicted in the three-dimensional spatial distribution functions, shown in Figure 4. We observe a high probability of finding the oxygen atoms of the anions close to the imidazolium ring of the cation. The anion interacts with the

cation mainly via the terminal oxygen atoms of the sulfate head, and the coordination occurs via the most acidic hydrogen atom in position C₂ but also through the hydrogen atoms in positions C₄ and C₅. We observe that the coordination of the anion is stronger when the length of the side chain of the anion increases, in good agreement with the results presented in the radial distribution functions depicted in Figure 3. Recently, Malberg et al.⁵⁴ using dispersion corrected ab initio molecular dynamics, have simulated the bulk and gas phase of the ionic liquid [C₂C₁im][C₂SO₄]. These authors observed that in the bulk phase the terminal atom of the anion interacts with the imidazolium ring of the cation, being situated above (below) of the ring: this establishes the dispersion interaction as the driving forces. This interaction is not present in the gas phase. We observe in panel a of Figure 4 the same feature: The terminal atom of the [C₂SO₄][−] anion can be found with high probability above (below) the imidazolium ring. Increasing the length of the side chain of the anion makes this interaction weaker (the green regions in the SDFs decrease in size), but it is still present in the IL. The good agreement between the results obtained in this work, using classical molecular simulations, and a nonpolarizable force field for the ionic liquids and the results of Malberg et al.⁵⁴ using dispersion corrected ab initio molecular dynamics (a technique where the electronic structure of the atoms is explicitly considered, and the interactions between the different atoms present on the simulation are calculated on the fly by means of a density functional theory calculation) allows us to validate the performance of the classical force field employed in this work.

To characterize the length scales of the polar and nonpolar regions, we use the static partial structure factors, $s_{ij}(k)$, corresponding to the partial RDFs, $g_{ij}(r)$, defined by Fourier transform according to eq 1, where ρ is the number density of the atomic sites considered.

$$S_{ij}(k) = 1 + \frac{4\pi\rho}{k} \int_0^\infty [g_{ij}(r) - 1] r \sin(rk) dr \quad (1)$$

Recently, Bodo et al.⁵⁵ and Macchiagodena et al.⁵⁶ were able to calculate the X-ray diffraction patterns of several imidazolium-based ionic liquids using molecular simulations, using the Debye scattering equations, where the atomic scattering factors for each atom contained in the system are accounted for. Therefore, the structure factors obtained from eq 1 differ quantitatively from the experimental X-ray diffraction patterns. Nevertheless, it is possible to directly compare qualitatively the results of our simulations with the experimental data obtained from X-ray measurements by Russina et al.³⁴ The results for the partial structure factors of several representative sites of the polar and nonpolar regions are presented in Figure 5. It is important to point out that the features observed at the very low k range are unreliable due to the limited box size. Peaks in the structure factors at values of $k \approx 1 \text{ \AA}^{-1}$ correspond to a wavelength of around $2\pi/1 = 6.2 \text{ \AA}$, i.e., to the distances between successive neighbor shells in the liquid structure. The existence of prepeaks in the structure factors indicates the presence of characteristic lengths that are larger than first-neighbor ion–ion contacts. Several works using both molecular simulation^{47,48} and experiments^{34,50–52} have highlighted the existence of such prepeaks in ionic liquids with alkyl side chains of intermediate length (in both cations and anions), indicating aggregation of the chains into nonpolar domains, while the charged head groups of the ions keep in close contact. The partial structure factors concerning the sulfur atoms of the

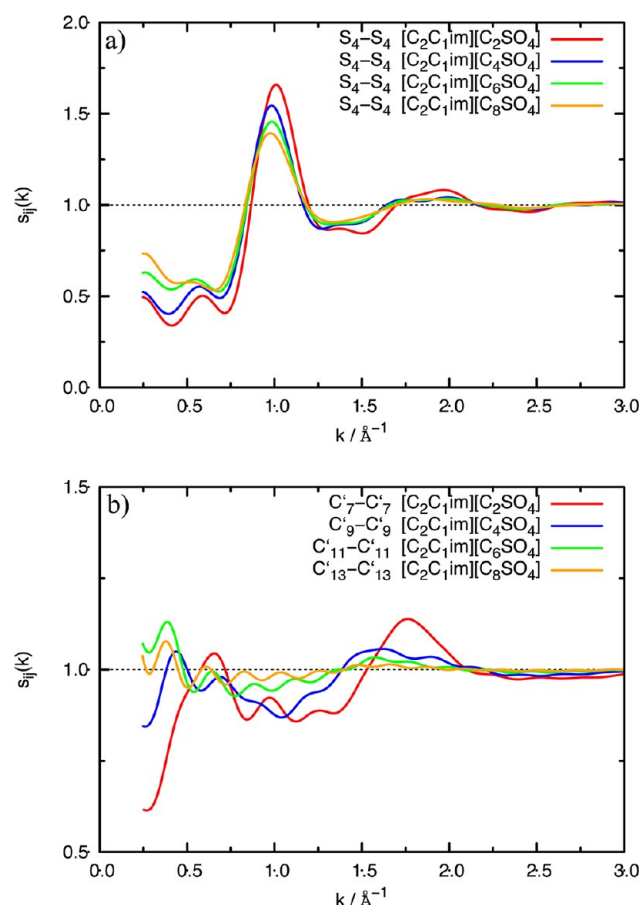


Figure 5. Static structure factors of representative atoms of the polar and nonpolar regions calculated from their radial distribution functions.

alkylsulfate anions show small peaks at about $0.54\text{--}0.60 \text{ \AA}^{-1}$. The peak wavenumbers corresponding to the length scales are presented in Table 1. The results suggest that the size of the

Table 1. Length Scales of the Polar/Nonpolar Domains Obtained from Analysis of the Static Structure Factors

| ionic liquid | peak wavenumber/ \AA^{-1} | length scale/ \AA |
|---|------------------------------------|----------------------------|
| Polar Domains | | |
| [C ₂ C ₁ im][C ₂ SO ₄] | 0.59 | 10.6 |
| [C ₂ C ₁ im][C ₄ SO ₄] | 0.57 | 11.0 |
| [C ₂ C ₁ im][C ₆ SO ₄] | 0.56 | 11.2 |
| [C ₂ C ₁ im][C ₈ SO ₄] | 0.54 | 11.6 |
| Nonpolar Domains | | |
| [C ₂ C ₁ im][C ₂ SO ₄] | 0.47 | 13.4 |
| [C ₂ C ₁ im][C ₄ SO ₄] | 0.44 | 14.3 |
| [C ₂ C ₁ im][C ₆ SO ₄] | 0.4 | 15.7 |
| [C ₂ C ₁ im][C ₈ SO ₄] | 0.38 | 16.5 |

polar regions are only slightly affected by the increase of the side chain of the anion. Coulombic interactions are dominant on ionic liquids, and their magnitude is only slightly dependent on the nonpolar part of the ions.⁵⁷ A slightly more interesting picture can be observed if we represent the partial structure factors of the terminal carbon atoms of the side chain of the alkylsulfate [C_nSO₄][−] anion, that provide an indication of the size of the nonpolar domains. We observe the existence of a small shoulder in the structure factor of the [C₂SO₄][−] at values

of $k \approx 0.47 \text{ \AA}^{-1}$. With increasing side chains of the anion, a distinct peak appears at values of $k \approx 0.44 \text{ \AA}^{-1}$, for the IL with the $[\text{C}_4\text{SO}_4]^-$ anion (Table 1). This peak shifts to lower k values for the ILs with the $[\text{C}_6\text{SO}_4]^-$ and $[\text{C}_8\text{SO}_4]^-$ anions, respectively, reflecting the size increase of the nonpolar regions in agreement with the snapshots presented in Figure 2. The results of our simulations are in good agreement with the experimental results obtained by Russina et al.³⁴ from X-ray measurements. These authors observe indications of nanosegregation for the IL $[\text{C}_2\text{C}_1\text{im}][\text{C}_2\text{SO}_4]$, in contrast with the results for different ionic liquids constituted by the same cation but different anions such as $[\text{PF}_6]^-$ or $[\text{NTf}_2]^-$. Russina et al.³⁴ estimated that the size increase of the nonpolar domains was $2.03 \text{ \AA}/\text{CH}_2$ unit. This value was comparable to the corresponding one obtained for other ILs, where the alkyl chain was bonded to the imidazolium ring of the cation.³⁴ The authors conclude that those values for the alkyl chain length dependence of the structural heterogeneities sizes reflect a characteristic organization of the nonpolar domains, with the alkyl chains stretching and not showing interdigitation. We observe a lower increase of the size of nonpolar domains with the number of CH_2 units for the studied alkylsulfate-based ionic liquids. A similar result was observed for Canongia Lopes and Pádua⁴⁷ for the family $[\text{C}_n\text{C}_1\text{im}][\text{PF}_6]$. To better understand the morphology of the nonpolar domains, we present in Figure S1 of the Supporting Information the radial distribution functions between the terminal carbon atoms of the anion and the other carbon atoms of the anion. We observe important peaks in the different RDFs, suggesting a complex situation. The ILs studied here do not form a clear laminar structure. These results, together with those of the X-ray experiments, suggest that further investigations on the structure of alkylsulfate-based ionic liquids are needed to clearly elucidate the structure of the nonpolar regions of the ILs. Computing the X-ray diffraction pattern from molecular simulation,^{55,56} will allow a quantitative comparison with the experimental X-ray data to be performed; nevertheless, this aspect is beyond the scope of the present article.

Ionic Liquid–Gas Interface. We present in Figure 6 the number density profile of the most representative atoms of the cation and anions. The alkyl side chains of both cations and anions tend to protrude toward the vacuum. An interesting feature is observed for the IL $[\text{C}_2\text{C}_1\text{im}][\text{C}_2\text{SO}_4]$, the terminal CH_3 group of the anion is found closer to the vacuum phase than that of the cation, which is found close to the bridging oxygen atom (O_5) of the anion. Low minima for the atoms of the side chain of the anion can be seen in the denser region (purple lines on panels a and b of Figure 6), where there is a maximum in the density of the atoms of the imidazolium rings of cation. The terminal oxygen atoms ($\text{O}_{1,2,3}$) of the anion are closer to the vacuum phase than the imidazolium ring of the cation. The increase of the side chain of the anion leads to interesting features in the liquid–vacuum interface of the IL. Thus, for $[\text{C}_2\text{C}_1\text{im}][\text{C}_8\text{SO}_4]$ we observe the existence of a layering in the ionic liquid below the surface, with significant fluctuations of the probability to find atoms belonging to the alkyl chain and to the imidazolium ring. A similar effect was observed previously⁴⁴ for $[\text{C}_8\text{C}_1\text{im}][\text{BF}_4]$. The side chains of the $[\text{C}_8\text{SO}_4]^-$ anion protrude toward the vacuum phase, leaving the oxygen atoms of the anion and those of the $[\text{C}_2\text{C}_1\text{im}]^+$ cation in an innermost region. The different atoms of the cation are found with high probability in the same region, suggesting a flat orientation of the cation with respect to the interface. The

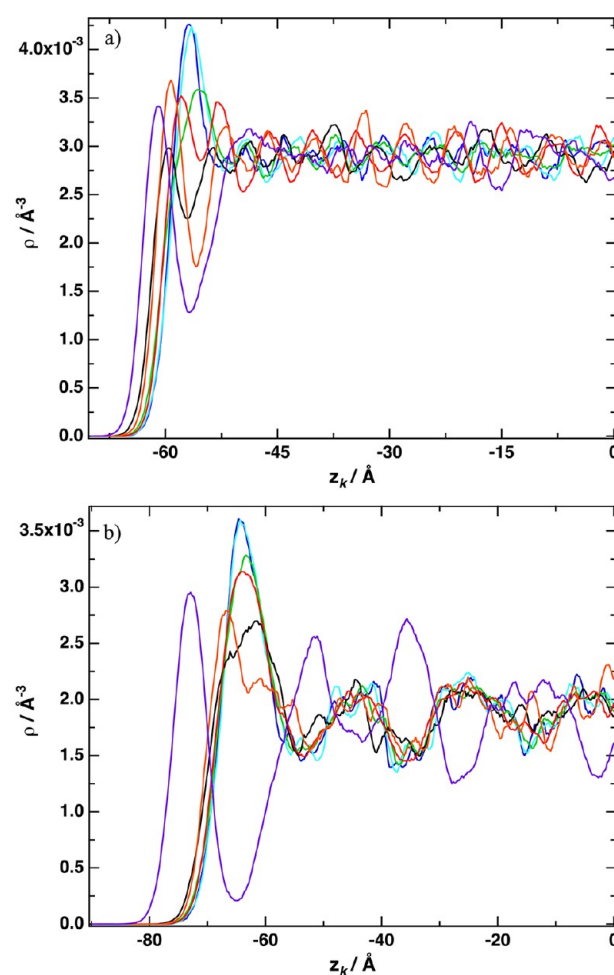


Figure 6. Number density profile of $[\text{C}_2\text{C}_1\text{im}][\text{C}_2\text{SO}_4]$ (upper panel) and $[\text{C}_2\text{C}_1\text{im}][\text{C}_8\text{SO}_4]$ (lower panel): blue line: C_2 ; cyan line: $\text{C}_{4,5}$; black line: C_7 ; green line: C_8 ; red line: $\text{O}_{1,2,3}$; orange line: O_5 ; purple line: C'_7 (panel a), C'_{13} (panel b).

simulation snapshot of Figure 7 shows a view looking down on the surface of the ionic liquids $[\text{C}_2\text{C}_1\text{im}][\text{C}_2\text{SO}_4]$ and $[\text{C}_2\text{C}_1\text{im}][\text{C}_8\text{SO}_4]$. It can be seen in panels a and c of Figure 7 that the alkyl chains do not cover totally the surface for both ionic liquids, therefore implying that the polar parts of the ionic liquids are accessible from above the surface. The structures of the polar and nonpolar regions of the ionic liquid are not strongly affected by the presence of a free surface, so the ionic liquid keeps its characteristic nanoscale heterogeneity.

We present in Figure 8 plots of the orientational ordering parameter, defined as the average of the second Legendre polynomial:

$$\langle P_2(\theta) \rangle = \left\langle \frac{1}{2}(3 \cos^2 \theta - 1) \right\rangle \quad (2)$$

In eq 2, θ is taken as the angle between a specific direction vector in the molecule-fixed frame and the surface normal z . The Legendre polynomial functions enable us to investigate the range and extent of orientation preferences at the interface. $P_2(\theta)$ ranges from 1 to -0.5 . A value of 1 implies that the two considered vectors are parallel, whereas a value of -0.5 indicates that they are perpendicular. We observe for both ionic liquids, $[\text{C}_2\text{C}_1\text{im}][\text{C}_2\text{SO}_4]$ and $[\text{C}_2\text{C}_1\text{im}][\text{C}_8\text{SO}_4]$, the imidazolium ring tends to adopt an orientation parallel to the

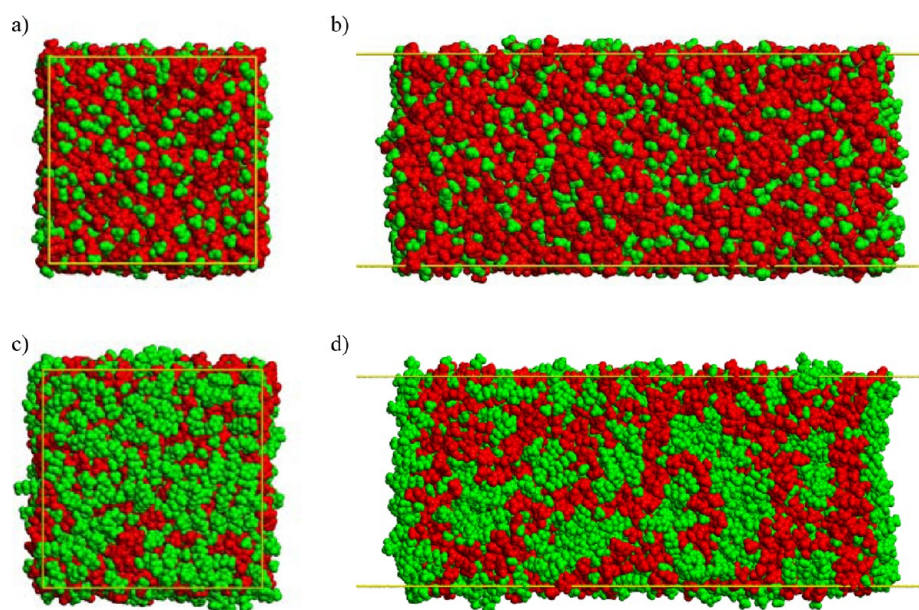


Figure 7. Snapshots of the simulation boxes. (a) and (b) [C₂C₁im][C₂SO₄], (c) and (d) [C₂C₁im][C₈SO₄].

interface, in agreement with the density profiles of Figure 6, where the different atoms of the imidazolium rings were present in the same region of the simulation box. For the IL [C₂C₁im][C₂SO₄], the side chains of the cations tend to align themselves with the normal direction to the interface (the angle is lower than 30°). The side chains of the anion form, in average, an angle between 30° and 45° with the normal to the interface. For the IL [C₂C₁im][C₈SO₄], the side chain of the anion preferentially forms angles lower than 30° with the normal to the interface, whereas the side chain of the cation is found preferentially forming angles around 45° with the *z* direction, in agreement with the density profiles presented in Figure 6.

From the density profiles of the different atoms of the cations and anions, it is possible to assess the charge distribution in the direction normal to the interface. Panel a of Figure 9 depicts the charge profile for the IL [C₂C₁im][C₂SO₄] along the direction normal to the interface. We observe an excess of positive charge in the liquid phase close to the interface, followed by a region of slightly negative charge. Strong oscillations of the charge profiles are observed, indicating the ordering effect of the interface. The fluctuations of the charge density profiles near the interface occur in characteristic sizes smaller than the size of the single ions, showing that there is no clear electrical double layer on the liquid–vacuum interface of the ionic liquid. According to the results of Figure 6, we observe that both cations and anions are present close to the surface; a weak segregation between cations and anions occurs, but there is not an electrical double layer. The electrostatic potential changes when crossing the surface of a liquid containing polar or charged entities. From the charge density profiles it is possible to evaluate the electrostatic potential Φ using Gauss' theorem:

$$\frac{d\Phi}{dz_k} = -\frac{1}{\epsilon_0} \int_{-\infty}^{z_k} \rho_q(z') dz' \quad (3)$$

where $\rho_q(z')$ is the charge density at the position z' . Panel b of Figure 9 shows the variation of the potential across the direction normal to the interface. Relative to the vacuum, the potential for the two considered ILs is negative, in agreement

with previous results⁴⁴ for imidazolium-based ionic liquids with alkyl and hydroxyl functionalized side chains. By analyzing the dependence of the potential in the liquid with the molecular structure, we can observe in panel b of Figure 9 that increasing the length of the side chain leads to less negative values of the potential. Bresme et al.⁵⁸ considered an ionic liquid consisting of spherical rigid ions interacting through the so-called “soft primitive model” (SPM), and they observed that ion size asymmetry results in charge separation at the liquid–vapor interface and therefore in a local violation of the electro-neutrality condition. The authors observed that an increase in size asymmetry results in an increase of the potential. Pensado et al.⁴⁴ observed in a previous work that increasing the side chain of the cation for ILs based on the [BF₄][−] anion, leads to more negative values of the potential, whereas for the ILs considered in this work, increasing the side chain of the alkylsulfate anion leads to less negative values of the potential, highlighting that not only the size of the ions but also the local ordering in the interfacial region plays a major role. The local ordering of the ions at the surface, the effective packing of the anion and cation in the interfacial region, together with the molecular structure of the ions are key parameters that control the values of the electrostatic potential at the surface. Thus, it is complex to predict the behavior of the potential considering only geometrical factors such as the shape of the ions and the effective packing at the interface (how the ions are structured in the interfacial region) can play also a major role. This aspect highlights the intrinsic complexity of ionic liquids and the difficulty to rationalize their properties in terms of the molecular structure.⁵⁹

To analyze the effect of the explicit interface on the structure of the ionic liquids, we calculated zone-resolved tangential pair distribution functions (TRDF) that will allow us to analyze the lateral structure of the interface. The TRDFs are defined by:

$$g_{ij}(r) \frac{\sum_{i,j} \delta(r - r_{ij})}{2\pi r dr \rho_{\text{region}} \Delta z}; \quad z_{ij} < \Delta z \quad (4)$$

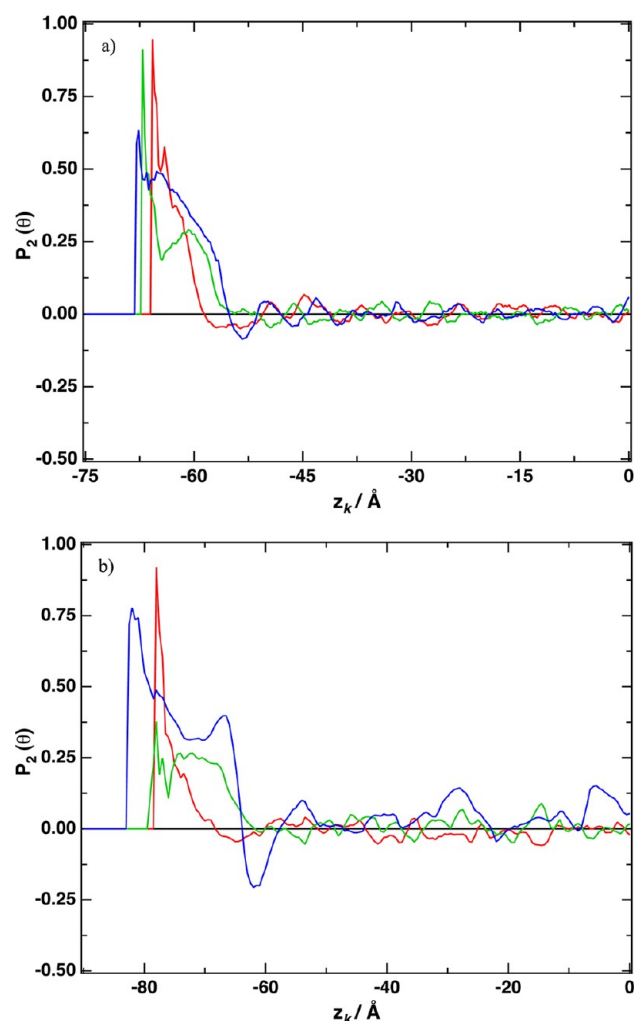


Figure 8. Orientational ordering parameter. θ is defined by the angle between the direction vectors and the surface normal. Red line: normal vector to the imidazolium ring; green line: N_1C_7 vector on $[C_2C_1im]^+$; blue line, upper panel: $O_5C'_7$ vector on the $[C_2SO_4]^-$ anion; and blue line, lower panel: $O_5C'_{13}$ vector on the $[C_8SO_4]^-$ anion.

where ρ_{region} is the average number density in each region which normalizes the corresponding TRDF to unity at infinite distance, and $r_{ij} = (x_{ij}^2 + y_{ij}^2)^{1/2}$ is a two-dimensional distance, parallel to the plane of the surface. $\Delta z = 5 \text{ \AA}$ is chosen to achieve significant statistical averages.

Figure 10 shows the TRDFs between several representative atoms of each ionic liquid. The TRDFs between the carbon atom C_2 of the imidazolium ring and the terminal oxygen atoms $O_{1,2,3}$ of the two anions are lower in the interfacial region than in the bulk region; this effect is more intense for the IL $[C_2C_1im][C_8SO_4]$. The presence of a discontinuity on the local density leads to a less ordered liquid phase near the interface, resulting in less efficient packing of cations and anions in the interfacial region. The most remarkable feature is the loss of the correlation between the terminal carbon atoms of the alkyl chains of both cations and anions in the interfacial region. The TRDFs between the terminal atoms of the $[C_2C_1im]^+$ cations and $[C_2SO_4]^-$ anions are, in the interfacial region, lower than 1, showing the lack of correlation of the side chains, in agreement with the snapshots of the simulation box presented in Figure 7. For the IL $[C_2C_1im][C_8SO_4]$, we observe that the TRDF between the terminal atoms of the $[C_8SO_4]^-$ anion shows in

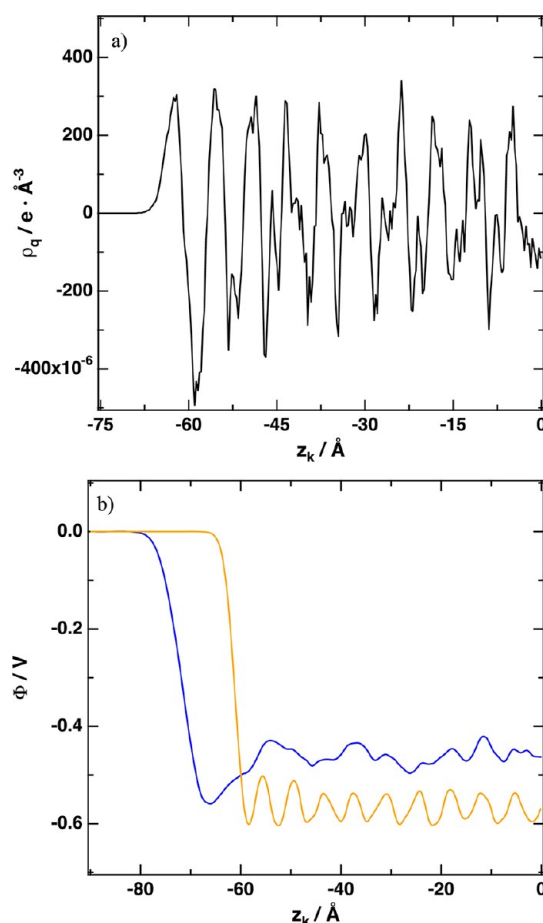


Figure 9. (a) Variation of the charge density for $[C_2C_1im][C_2SO_4]$. (b) Electrostatic potential for $[C_2C_1im][C_2SO_4]$: orange line and $[C_2C_1im][C_8SO_4]$: blue line.

the interfacial region a small peak at distances around 5 \AA , but much lower than that observed in the bulk. The outer region of the interface is composed mainly of the side chains of the anions, but their correlation is weak.

We present in Table 2 the values of the surface tension for the two ionic liquids studied, using the Kirkwood–Buff and Irving–Kirkwood expressions. A good agreement between both methods is observed. Panel a of Figure 11 shows the profiles of the surface tension for the ionic liquid $[C_2C_1im][C_2SO_4]$ across the direction normal to the interface; similar behavior is observed for the ionic liquid $[C_2C_1im][C_8SO_4]$. The contributions to the surface tension for a system in mechanical equilibrium should come from the interfacial regions and not from the isotropic bulk region, as it is pointed out in a number of molecular simulation studies^{60–63} on surface tension, concerning different systems. The profiles of pseudolocals surface tension should increase in a similar way in the two interfacial regions, and remain constant in the bulk phases, as required for a system in mechanical equilibrium. As it was observed previously for different ionic liquids,^{44,45} the dispersion–repulsion contribution to the surface tension (calculated from the Irving–Kirkwood approach) is negative, whereas the electrostatic contribution is positive. Panel b of Figure 11 depicts the contribution of the long-range correction to the surface tension for $[C_2C_1im][C_8SO_4]$. Again, there is no contribution of the long-range correction to the surface tension coming from the bulk, since the integral of $\gamma_z(z_k)$ is flat in this

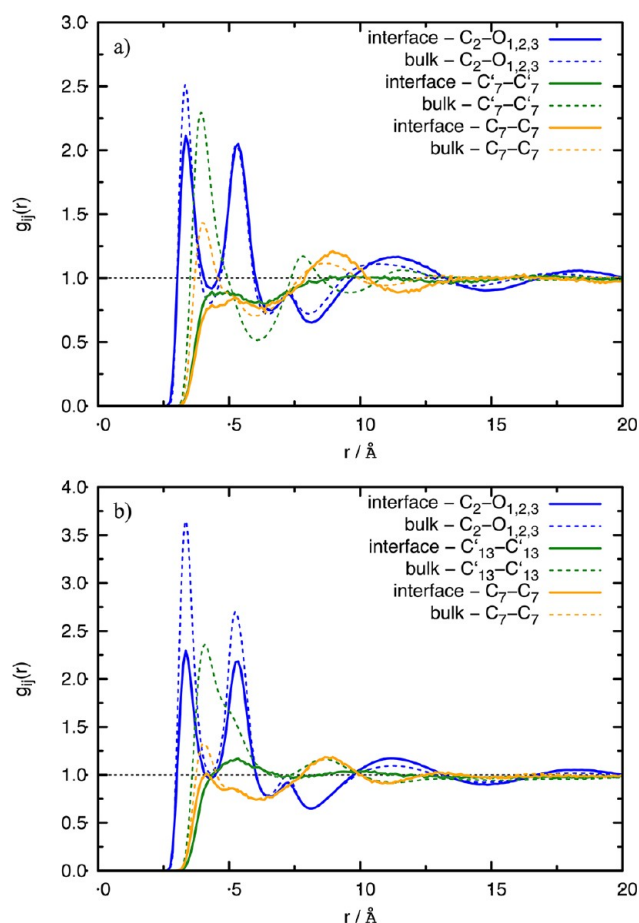


Figure 10. Tangential radial distribution functions (TRDF) of individual regions for several representative pairs of atoms in the interfacial (solid lines) and bulk regions (dashed lines): (a) $[\text{C}_2\text{C}_1\text{im}][\text{C}_2\text{SO}_4]$: blue line: $\text{C}_2\text{--O}_{1,2,3}$; green line: $\text{C}_7'\text{--C}_7$; orange line: $\text{C}_7\text{--C}_7$. (b) $[\text{C}_2\text{C}_1\text{im}][\text{C}_8\text{SO}_4]$: blue line: $\text{C}_2\text{--O}_{1,2,3}$; green line: $\text{C}_{13}'\text{--C}_{13}$; orange line: $\text{C}_7\text{--C}_7$.

Table 2. Surface Tension ($\text{mN}\cdot\text{m}^{-1}$) for the Studied Ionic Liquids Calculated from MD Simulations Using the Different Operational Expressions at $T = 423\text{ K}^a$

| | $[\text{C}_2\text{C}_1\text{im}][\text{C}_2\text{SO}_4]$ | $[\text{C}_2\text{C}_1\text{im}][\text{C}_8\text{SO}_4]$ |
|------------------------|--|--|
| γ_{KB} | 36.6 ± 3.9 | 20.1 ± 2.2 |
| γ_{IB} | 34.6 ± 3.9 | 22.3 ± 2.4 |
| γ_{LRC} | 2.4 | 1.8 |
| $\langle\gamma\rangle$ | 38.0 ± 3.9 | 23.0 ± 2.4 |

^a $\langle\gamma\rangle$ is averaged over KB and IK methods.

region. The long-range corrections, γ_{LRC} , to the surface tension account for around 10% of the total (see Table 2), and this underlines the need for considering this correction carefully. It is possible to relate the surface tension of the ionic liquids to the structure at the free surface. The ionic liquids behave as surfactants, so when the length of the alkyl side chain is increased, the more favorable configurations correspond to alkyl chains in the vacuum side, leading to a decrease in the surface tension, as observed in this work.

The force field used in this work was not adjusted to surface properties; therefore, the calculation of surface tension is also a test of the transferability of the force field. Restolho et al.⁶⁴ investigated the surface tension of the IL $[\text{C}_2\text{C}_1\text{im}][\text{C}_2\text{SO}_4]$ from 298 to 453 K, using the pending drop method. Yang et

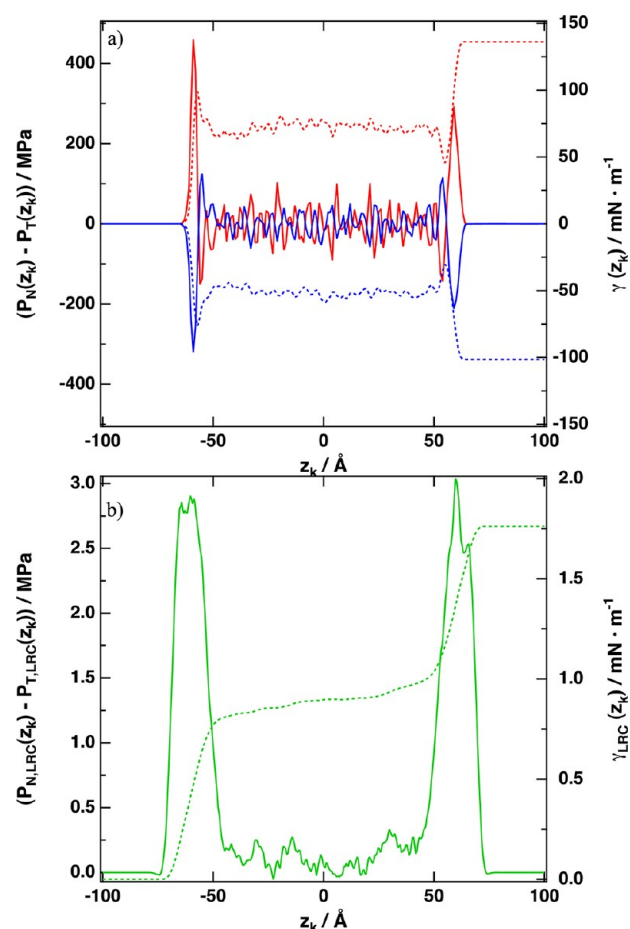


Figure 11. (a) $p_{\text{N}}(z_k) - p_{\text{T}}(z_k)$ for the Lennard-Jones (red curve) and the electrostatic part of the potential (blue curve) as a function of z_k for $[\text{C}_2\text{C}_1\text{im}][\text{C}_2\text{SO}_4]$. The dashed lines correspond to the integral as a function of z (right axis); (b) $p_{\text{N}}(z_k) - p_{\text{T}}(z_k)$ for the long-range corrections as a function of z_k for $[\text{C}_8\text{C}_1\text{im}][\text{C}_8\text{SO}_4]$. The dashed lines correspond to the integral as a function of z_k (right axis).

al.⁶⁵ measured the surface tension of this IL from 278.15 to 328.15 K, using the maximum bubble pressure method. Gómez et al.,⁶⁶ using the drop weight method, reported surface tension data for the same IL in the range of 283.15–313.15 K. Wandschneider et al.,⁶⁷ using the drop pending method, measured the surface tension of $[\text{C}_2\text{C}_1\text{im}][\text{C}_2\text{SO}_4]$ from 278.75 to 328.15 K, Fernández et al.,⁶⁸ using the drop weight method, reported values of the surface tension of this IL from 303.15 to 333.15 K. Finally, Nieto de Castro et al.⁶⁹ measured the surface tension from 293.15 to 332.15 K, using the Wilhelmy plate method. The results of our simulations agree with the extrapolated data with deviations of 1%, −7%, 2%, 2%, −9%, and −7%, respectively. Hasse et al.⁷⁰ measured the surface tension of the $[\text{C}_2\text{C}_1\text{im}][\text{C}_8\text{SO}_4]$ at 293 K, finding a value of 31 $\text{mN}\cdot\text{m}^{-1}$. It is therefore not possible to compare the experimental value of the surface tension for this IL with the results of our simulations. Nevertheless, the experiments⁷¹ show that, at constant temperature, increasing the side-chain length (anion) of the alkylsulfate-based ionic liquids based on the IL $[\text{C}_2\text{C}_1\text{im}]^+$ cation leads to a decrease of the values of the surface tension, in good agreement with our simulations. The comparison of the surface tension values calculated from molecular simulations and the experimental values allows us to conclude that the atomistic force field and the simulation

techniques used in the present work are able to predict the surface tension of ionic liquids within a maximum deviation of $\pm 10\%$.

CONCLUSIONS

Using molecular simulation we were able to explore the relation between the molecular structure of several imidazolium ionic liquids, linked with alkylsulfate anions (with different side-chain lengths) and the structure of the polar and nonpolar regions present in these ILs. The results of our simulations concerning the characteristic size of the nonpolar regions agree qualitatively with the experimental data of Russina et al.³⁴ using X-ray measurements. We observe that dispersion forces, correctly described with the classical force field used in this work, explain the presence of the side chain of the anion close to the imidazolium ring of the cation, this effect being less evident when the side chain of the anion increases. Using molecular simulation it is also possible to explore the structure of the ionic liquid–gas interface. We observe that the ionic liquid with long side chains behaves like a surfactant, with the side chains pointing toward the vacuum, whereas the cations adopt orientations with the imidazolium ring parallel to the surface. The values of the surface tension obtained from the simulations are in good agreement with the experimental data, and the trend of this property with the molecular structure of the ions is well reproduced. Molecular simulation can be used to assist the design of ionic liquids with specific surface properties.

ASSOCIATED CONTENT

Supporting Information

Radial distribution functions between the terminal carbon atoms of the anion and the other carbon atoms of the anion. This material is available free of charge via the Internet at <http://pubs.acs.org>.

AUTHOR INFORMATION

Corresponding Author

*E-mail: patrice.malfreyt@univ-bpclermont.fr (P.M.); alfonso.pensado@uni-leipzig.de (A.S.P.)

Notes

The authors declare no competing financial interest.

ACKNOWLEDGMENTS

This work was supported by the Spanish Science and Technology Ministry (CTQ2008-6498-C02-01 and CTQ2011-23925 projects) and the DFG, in particular by Projects KI-768/7-1 and KI-768/5-3 from the SPP-IL program. The participation of A.S.P. was made possible by a postdoctoral fellowship granted by the DFG through the SPP-IL program. Computer time from the “Centro de Supercomputación de Galicia” (CESGA) is acknowledged gratefully.

REFERENCES

- (1) Hallett, J. P.; Welton, T. *Chem. Rev.* **2011**, *111*, 3508–3576.
- (2) Brehm, M.; Weber, H.; Pensado, A. S.; Stark, A.; Kirchner, B. *Phys. Chem. Chem. Phys.* **2012**, *14*, 5030–5044.
- (3) Zahn, S.; Uhlig, F.; Thar, J.; Spickermann, C.; Kirchner, B. *Angew. Chem., Int. Ed.* **2008**, *47*, 3639–3641.
- (4) Izgorodina, E. I. *Phys. Chem. Chem. Phys.* **2011**, *13*, 4189–4207.
- (5) Izgorodina, E. I.; MacFarlane, D. R. *J. Phys. Chem. B* **2011**, *115*, 14659–14667.
- (6) Lehmann, S. B. C.; Roatsch, M.; Schöppke, M.; Kirchner, B. *Phys. Chem. Chem. Phys.* **2010**, *12*, 7473–7486.
- (7) Morrow, T. I.; Maginn, E. J. *J. Phys. Chem. B* **2002**, *106*, 12807–12813.
- (8) Earle, M. J.; Esperança, J. M. S. S.; Gilea, M. A.; Canongia Lopes, J. N.; Rebelo, L. P. N.; Magee, J. W.; Seddon, K. R.; Widegren, J. A. *Nature* **2006**, *439*, 831–834.
- (9) Rebelo, L. P. N.; Canongia Lopes, J. N.; Esperança, J. M. S. S.; Filipe, E. J. *Phys. Chem. B* **2005**, *109*, 6040–6043.
- (10) Bayley, P. M.; Best, A. S.; MacFarlane, D. R.; Forsyth, M. *ChemPhysChem* **2011**, *12*, 823–827.
- (11) Lane, G. H.; Best, A. S.; MacFarlane, D. R.; Forsyth, M.; Bayley, P. M.; Hollenkamp, A. F. *Electrochim. Acta* **2010**, *55*, 8947–8952.
- (12) Simons, T. J.; Torriero, A. A. J.; Howlett, P. C.; MacFarlane, D. R.; Forsyth, M. *Electrochem. Commun.* **2012**, *18*, 119–122.
- (13) Almantariotis, D.; Stevanovic, S.; Fandino, O.; Pensado, A. S.; Padua, A. A. H.; Coxam, J. Y.; Costa Gomes, M. F. *J. Phys. Chem. B* **2012**, *116*, 7728–7738.
- (14) Almantariotis, D.; Gefflaut, T.; Pádua, A. A. H.; Coxam, J.-Y.; Costa Gomes, M. F. *J. Phys. Chem. B* **2010**, *114*, 3608–3617.
- (15) Anthony, J. L.; Anderson, J. L.; Maginn, E. J.; Brennecke, J. F. *J. Phys. Chem. B* **2005**, *109*, 6366–6374.
- (16) Deng, Y.; Morrissey, S.; Gathergood, N.; Delort, A. M.; Husson, P.; Costa Gomes, M. F. *ChemSusChem* **2010**, *3*, 377–385.
- (17) Li, R.; Xing, H.; Yang, Q.; Zhao, X.; Su, B.; Bao, Z.; Yang, Y.; Ren, Q. *Ind. Eng. Chem. Res.* **2012**, *51*, 8588–8597.
- (18) Zhao, W.; He, G.; Nie, F.; Zhang, L.; Feng, H.; Liu, H. *J. Membr. Sci.* **2012**, *411*, 73–80.
- (19) Mokrushin, V.; Assenbaum, D. I.; Paape, N.; Gerhard, D.; Mokrushina, L.; Wasserscheid, P.; Arlt, W.; Kistenmacher, H.; Neuendorf, S.; Goeke, V. *Chem. Eng. Technol.* **2010**, *33*, 63–73.
- (20) Lei, Z. G.; Arlt, W.; Wasserscheid, P. *Fluid Phase Equilib.* **2006**, *241*, 290–299.
- (21) Campbell, P. S.; Santini, C. C.; Bouchu, D.; Fenet, B.; Philippot, K.; Chaudret, B.; Padua, A. A. H.; Chauvin, Y. *Phys. Chem. Chem. Phys.* **2010**, *12*, 4217–4223.
- (22) Salas, G.; Podgorsek, A.; Campbell, P. S.; Santini, C. C.; Padua, A. A. H.; Costa Gomes, M. F.; Philippot, K.; Chaudret, B.; Turmine, M. *Phys. Chem. Chem. Phys.* **2011**, *13*, 13527–13536.
- (23) Dupont, J.; Scholten, J. D. *Chem. Soc. Rev.* **2010**, *39*, 1780–1804.
- (24) Precht, M. H. G.; Campbell, P. S.; Scholten, J. D.; Fraser, G. B.; Machado, G.; Santini, C. C.; Dupont, J.; Chauvin, Y. *Nanoscale* **2010**, *2*, 2601–2606.
- (25) Gutel, T.; Santini, C. C.; Philippot, K.; Padua, A. A. H.; Pelzer, K.; Chaudret, B.; Chauvin, Y.; Basset, J. M. *J. Mater. Chem.* **2009**, *19*, 3624–3631.
- (26) Pereiro, A. B.; Deive, F. J.; Esperança, J. M. S. S.; Rodriguez, A. *Fluid Phase Equilib.* **2010**, *294*, 49–53.
- (27) Holbrey, J. D.; Reichert, W. M.; Swatloski, R. P.; Broker, G. A.; Pitner, W. R.; Seddon, K. R.; Rogers, R. D. *Green Chem.* **2002**, *4*, 407–413.
- (28) Domanska, U.; Laskowska, M. *J. Solution Chem.* **2008**, *37*, 1271–1287.
- (29) Costa, A. J. L.; Esperança, J. M. S. S.; Marrucho, I. M.; Rebelo, L. P. N. *J. Chem. Eng. Data* **2011**, *56*, 3433–3441.
- (30) Gaciño, F. M.; Regueira, T.; Lugo, L.; Comuñas, M. J. P.; Fernández, J. J. *J. Chem. Eng. Data* **2011**, *56*, 4984–4999.
- (31) Deng, Y.; Besse-Hoggan, P.; Sancelme, M.; Delort, A. M.; Husson, P.; Costa Gomes, M. F. *J. Hazard. Mater.* **2011**, *198*, 165–174.
- (32) Wilfred, C. D.; Kiat, C. F.; Man, Z.; Bustam, M. A.; Mutalib, M. I. M.; Phak, C. Z. *Fuel Process. Technol.* **2012**, *93*, 85–89.
- (33) Pereiro, A. B.; Deive, F. J.; Esperança, J. M. S. S.; Rodriguez, A. *Fluid Phase Equilib.* **2010**, *291*, 13–17.
- (34) Russina, O.; Gontrani, L.; Fazio, B.; Lombardo, D.; Triolo, A.; Caminiti, R. *Chem. Phys. Lett.* **2010**, *493*, 259–262.
- (35) Martinez, I. S.; Santos, C.; Baldelli, S. *ChemPhysChem* **2012**, *13*, 1818–1824.
- (36) Canongia Lopes, J. N.; Pádua, A. A. H.; Shimizu, K. *J. Phys. Chem. B* **2008**, *112*, 5039–5046.
- (37) Canongia Lopes, J. N.; Deschamps, J.; Padua, A. A. H. *J. Phys. Chem. B* **2004**, *108*, 2038–2047.

- (38) Jorgensen, W. L.; Maxwell, D. S.; Tirado-Rives, J. *J. Am. Chem. Soc.* **1996**, *118*, 11225–11236.
- (39) Cornell, W. D.; Cieplak, P.; Bayly, C. I.; Gould, I. R.; Merz, K. M.; Fergusin, D. M.; Spellmeyer, D. C.; Fox, T.; Caldwell, J. W.; Kollman, P. A. *J. Am. Chem. Soc.* **1995**, *117*, 5179–5197.
- (40) Smith, W.; Forester, T. R. *DL_POLY Molecular Simulation Package*; CSE Department, STFC Daresbury Laboratory: Daresbury, Warrington, U.K., 2007.
- (41) Gloor, G. J.; Jackson, G.; Blas, F. J.; De-Miguel, E. *J. Chem. Phys.* **2005**, *123*, 134703.
- (42) Irving, J. H.; Kirkwood, J. G. *J. Chem. Phys.* **1950**, *18*, 817–829.
- (43) Kirkwood, J. G.; Buff, F. P. *J. Chem. Phys.* **1949**, *17*, 338–343.
- (44) Pensado, A. S.; Costa Gomes, M. F.; Canongia Lopes, J. N.; Malfreyt, P.; Padua, A. A. H. *Phys. Chem. Chem. Phys.* **2011**, *13*.
- (45) Pensado, A. S.; Malfreyt, P.; Pádua, A. A. H. *J. Phys. Chem. B* **2009**, *113*, 14708–14718.
- (46) Wang, Y.; Voth, G. A. *J. Am. Chem. Soc.* **2005**, *127*, 12192–12193.
- (47) Canongia Lopes, J. N.; Pádua, A. A. H. *J. Phys. Chem. B* **2006**, *110*, 3330–3335.
- (48) Pensado, A. S.; Padua, A. A. H.; Costa Gomes, M. F. *J. Phys. Chem. B* **2011**, *115*, 3942–3948.
- (49) Russina, O.; Triolo, A.; Gontrani, L.; Caminiti, R. *J. Phys. Chem. Lett.* **2012**, *3*, 27–33.
- (50) Russina, O.; Triolo, A.; Gontrani, L.; Caminiti, R.; Xiao, D.; Hines, L. G., Jr; Bartsch, R. A.; Quitevis, E. L.; Plechkova, N.; Seddon, K. R. *J. Phys.: Condens. Matter* **2009**, *21*, 424121–424129.
- (51) Triolo, A.; Russina, O.; Bleif, H.-J.; Di Cola, E. *J. Phys. Chem. B* **2007**, *111*, 4641–4644.
- (52) Triolo, A.; Russina, O.; Fazio, B.; Triolo, R.; Di Cola, E. *Chem. Phys. Lett.* **2008**, *457*, 362–365.
- (53) Padua, A. A. H.; Costa Gomes, M. F.; Canongia Lopes, J. N. *Acc. Chem. Res.* **2007**, *40*, 1087–1096.
- (54) Malberg, F.; Pensado, A. S.; Kirchner, B. *Phys. Chem. Chem. Phys.* **2012**, *14*, 12079–12082.
- (55) Bodo, E.; Gontrani, L.; Caminiti, R.; Plechkova, N. V.; Seddon, K. R.; Triolo, A. *J. Phys. Chem. B* **2010**, *114*, 16398–16407.
- (56) Macchiagodena, M.; Gontrani, L.; Ramondo, F.; Triolo, A.; Caminiti, R. *J. Chem. Phys.* **2011**, *134*, 114521.
- (57) Shimizu, K.; Costa Gomes, M. F.; Padua, A. A. H.; Rebelo, L. P. N.; Canongia Lopes, J. N. *J. Mol. Struct. (THEOCHEM)* **2010**, *946*, 70–76.
- (58) Bresme, F.; González-Melchor, M.; Alejandre, J. *J. Phys.: Condens. Matter* **2005**, *17*, S3301–S3307.
- (59) Blesic, M.; Swadzba-Kwasny, M.; Belhocine, T.; Gunaratne, H. Q. N.; Canongia Lopes, J. N.; Gomes, M. F. C.; Padua, A. A. H.; Seddon, K. R.; Rebelo, L. P. N. *Phys. Chem. Chem. Phys.* **2009**, *11*, 8939–8948.
- (60) Biscay, F.; Ghoufi, A.; Goujon, F.; Lachet, V.; Malfreyt, P. *J. Chem. Phys.* **2009**, *130*, 184710.
- (61) Biscay, F.; Ghoufi, A.; Lachet, V.; Malfreyt, P. *J. Phys. Chem. B* **2011**, *115*, 8670–8683.
- (62) Neyt, J. C.; Wender, A.; Lachet, V.; Malfreyt, P. *J. Phys. Chem. C* **2012**, *116*, 10563–10572.
- (63) Ghoufi, A.; Goujon, F.; Lachet, V.; Malfreyt, P. *J. Chem. Phys.* **2008**, *128*, 154716.
- (64) Restolho, J.; Mata, J. L.; Saramago, B. *J. Colloid Interface Sci.* **2009**, *340*, 82–86.
- (65) Yang, J. Z.; Lu, X. M.; Gui, J. S.; G., X. W. *Green Chem.* **2004**, *6*, 541–543.
- (66) Gómez, E.; González, B.; Calvar, N.; Tojo, E.; Domínguez, A. *J. Chem. Eng. Data* **2006**, *51*, 2096–2102.
- (67) Wandschneider, A.; Lehmann, J. K.; Heintz, A. *J. Chem. Eng. Data* **2008**, *53*, 596–599.
- (68) Fernández, A.; García, J.; Torrecilla, J. S.; Olié, M.; Rodríguez, F. *J. Chem. Eng. Data* **2008**, *53*, 1518–1522.
- (69) Nieto de Castro, C. A.; Langa, E.; Morais, A. L.; Matos Lopes, M. L.; Lourenço, M. J. V.; Santos, F. J. V.; Santos, M. S. C. S.; Canongia Lopes, J. N.; Veiga, H. I. M.; Macatrão, M.; et al. *Fluid Phase Equilib.* **2010**, *294*, 157–179.
- (70) Hasse, B.; Lehmann, J. K.; Assenbaum, D. I.; Wasserscheid, P.; Leipertz, A.; Fröba, A. P. *J. Chem. Eng. Data* **2009**, *54*, 2576–2583.
- (71) Tariq, M.; Freire, M. G.; Saramago, B.; Coutinho, J. A. P.; Canongia Lopes, J. N.; Rebelo, L. P. N. *Chem. Soc. Rev.* **2012**, *41*, 829–868.